This is a repository copy of *GOTO065054+593624: An 8.5 mag amplitude dwarf nova identified in real time via Kilonova Seekers*.

White Rose Research Online URL for this paper:
https://eprints.whiterose.ac.uk/228938/

Version: Published Version

Takedown
If you consider content in White Rose Research Online to be in breach of UK law, please notify us by emailing eprints@whiterose.ac.uk including the URL of the record and the reason for the withdrawal request.

Astronomy & Astrophysics

GOTO065054+593624: An 8.5 mag amplitude dwarf nova identified in real time via Kilonova Seekers

T. L. Killestein[1,2,★] , G. Ramsay[3] , M. Kennedy[4] , L. Kelsey[5] , D. Steeghs[2] , S. Littlefair[6] , B. Godson[2] ,
J. Lyman[2] , M. Pursiainen[2] , B. Warwick[2] , C. Krawczyk[7] , L. K. Nuttall[7] , E. Wickens[7] , S. D. Alexandrov[8,9] ,
C. M. da Silva[8,10,11] , R. Leadbeater[12] , K. Ackley[2] , M. J. Dyer[6] , F. Jiménez-Ibarra[13] , K. Ulaczyk[2] ,
D. K. Galloway[13] , V. S. Dhillon[6,14] , P. O'Brien[15] , K. Noysena[16] , R. Kotak[1] , R. P. Breton[17] , E. Pallé[14] ,
D. Pollacco[2] , A. Kumar[2,18] , D. O'Neill[2] , T. Butterley[19] , R. Wilson[19] , S. Mattila[1,20] , A. Sahu[2] , R. Starling[15] ,
C. Y. Wang[21] , Q. Liu[22] , A. Li[23,24] , Z. Dai[25,26] , H. Feng[27] , W. Yuan[28,29] , R. Billington[8] , A. G. Bull[8,30,31] ,
S. Gaudenzi[8,10] , V. Gonano[8] , H. Krawczyk[8] , M. T. Mazzucato[8,31,32] , A. Pasqua[8] , J. A. da Silva Campos[8,33] ,
M. Torres-Guerrero[8] , N. N. Antonov[34] , S. J. Bean[12] , E. T. Boeneker[10] , S. M. Brincat[10] , G. S. Darlington[12,10] ,
F. Dubois[35,36] , F.-J. Hambsch[36,10,37,38] , D. Messier[10,39] , A. Oksanen[10,40] , G. Poyner[12] , F. D. Romanov[10,41] ,
I. D. Sharp[12] , T. Tordai[42] , T. Vanmunster[10,39] , and K. Wenzel[38]

(Affiliations can be found after the references)

ABSTRACT

Dwarf novae are astrophysical laboratories for probing the nature of accretion, binary mass transfer, and binary evolution, but their diverse observational characteristics continue to challenge our theoretical understanding. We here present the discovery of and subsequent observing campaign on GOTO065054+593624 (hereafter GOTO0650), a dwarf nova of the WZ Sge type that was discovered in real-time by citizen scientists via the Kilonova Seekers citizen science project. The nova has an outburst amplitude of 8.5 mag. An extensive dataset charts the photometric and spectroscopic evolution of this object, and it covers the 2024 superoutburst. GOTO0650 shows an absence of visible emission lines during the high state, strong H and barely detected He II emission, and high-amplitude echo outbursts on a rapidly decreasing timescale. The comprehensive dataset we present marks GOTO0650 as a candidate period bouncer, and it highlights the important contribution made by citizen scientists to the study of Galactic transients.

Key words. binaries: close – stars: dwarf novae – novae, cataclysmic variables

1. Introduction

Cataclysmic variables (CVs) are the most populous type of accreting binaries and represent the end state of binary star evolution, in which the more massive stellar component is a white dwarf (WD) and the secondary is a late-type main-sequence star, or a brown dwarf. At some point in the past, their WD progenitor star evolved off the main sequence, and its expanding outer envelope engulfed a main-sequence companion star. During a short-lived common-envelope episode, angular momentum was removed efficiently from the binary with the ejection of the envelope, leaving a close pair with a separation of a few solar radii and an orbital period of ∼6–10 hours (Warner 2003).

Gradually, angular momentum is lost from the system through a combination of the stellar wind from the secondary star and gravitational-wave radiation, which results in the secondary star filling its Roche lobe and initiating ballistic mass transfer to the WD through the inner Lagrange point L1, forming an accretion disc around the WD if its magnetic field is ≲1 MG. Low-luminosity states correspond to intervals with a low accretion rate, where accreting matter accumulates in the outer disc. When the disc density reaches a certain threshold, the disc becomes ionised and switches viscosity state. The ensu-

ing outburst manifests as an episode with a high accretion rate and high luminosity and causes the cataclysmic phenomenon. These high-amplitude outbursts enabled the first detection of a CV in 1855 (Hind 1856). Since then, amateur astronomers (perhaps better known today as citizen scientists) have continued to make an important contribution to studying these systems (e.g. Jensen et al. 1995; Shears 2018).

Angular momentum continues to be lost from the system until the late-type star becomes fully convective and magnetic braking is thought to be significantly reduced. The secondary detaches from its Roche lobe, and accretion ceases until the continued angular momentum loss through gravitational waves causes the binary orbit to shrink, and accretion restarts. This results in the so-called period gap (see Schreiber et al. 2024 for a recent summary). As the CV orbit shrinks further, a point (known as the period minimum, which is predicted to be ∼78 min) is reached when the core of the late-type star becomes a brown dwarf. At this point, further mass loss from the donor then causes its radius to stop contracting, and to conserve angular momentum, the orbital period starts to increase, and thus the CV becomes a 'period bouncer', that is, a CV system that evolved beyond the period minimum (see Knigge et al. 2011 for a review of the evolution of CVs).

The number of CVs near the predicted period minimum is a sensitive test of binary evolution models. These models

predict that a significant fraction (40–70%) of all galactic CVs are period bouncers (e.g. Kolb 1993; Howell et al. 2001; Goliasch & Nelson 2015; Belloni et al. 2020): The problem is that very few such systems are known (e.g. Pala et al. 2018; Inight et al. 2023), likely because it is difficult to determine for systems around the period minimum whether they still have to reach the minimum, or if their period is now becoming longer and the system is therefore post-minimum.
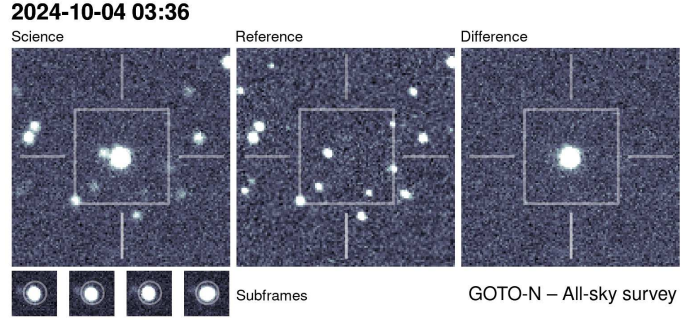
One class of CVs with orbital periods close to the period minimum is the WZ Sge type (see Kato 2015, for a review), which are good candidates for period bouncers. WZ Sge systems show high-amplitude outbursts (typically greater than 6 mag) that recur on a timescale of years or decades. This is much longer than dwarf nova outbursts in systems with longer orbital periods. The reason is their very low-mass transfer rate (e.g. 10^{15} g/s (1.6×10^{-10} $M_\odot$/yr) for WZ Sge stars compared to 10^{16} g/s (1.6×10^{-9} $M_\odot$/yr) for SU UMa stars; Osaki & Meyer 2002). They also display a periodic modulation in the long decline from maximum that is known as superhumps, with a period slightly longer than the orbital period. Some outbursts show evidence of echo outbursts that occur two to three weeks after the peak and are excellent tests of accretion instability models (e.g. Patterson et al. 2002).

In recent years, optical wide-field surveys have discovered more WZ Sge systems than ever before (e.g. Tampo et al. 2021). This filled out the parameter space of these systems and unveiled unique examples. In this paper, we present observations and an initial analysis of a new WZ Sge system that was discovered using the Gravitational-wave Optical Transient Observer (GOTO) all-sky survey, and was first identified via the Kilonova Seekers citizen science project in October 2024.

2. Discovery

GOTO065054+593625 (hereafter GOTO0650) was first detected during the all-sky survey of the Gravitational-wave Optical Transient Observer (GOTO; Dyer et al. 2018, 2024; Steeghs et al. 2022) in an image taken on 2024 October 4 03:36:36 UT by GOTO-North on La Palma. The source was extremely bright at the discovery, with a GOTO L-band (400–700 nm) magnitude of 13.37 ± 0.01, and it was located at $\alpha = 06^h50^m54.49^s$, $\delta = +59°36'24.51''$ (J2000) (Killestein et al. 2024a). The field was last visited ≈ 2 d prior to discovery by GOTO, with a non-detection of this source down to $L < 20.2$ mag. There was a further non-detection 5.5 h later with the All-Sky Automated Survey for Supernovae (ASAS-SN; Shappee et al. 2014), $g > 17.4$ mag. This constrains the outburst to within a time window of 1.8 days[1].

Notably, GOTO0650 was first identified by citizen scientists working via the Kilonova Seekers (Killestein et al. 2024b) project on the Zooniverse platform. The observations by the volunteers reached the required threshold for promoting the object as real approximately 3.5 hours after discovery. Ninety percent of the volunteers who viewed the candidate image voted the object to be real and astrophysical. Because of the primarily extragalactic focus of GOTO team vetting, this object had previously been put on hold in the 'pending' source list of the internal GOTO Marshall (Lyman et al., in prep.), awaiting further information because it might be associated with a faint point source identified in the Panoramic Survey Tele-

---

[1] All times in this paper are given relative to the GOTO discovery epoch (MJD 60 587.15), which is likely close to the time of maximum light given the strong rise constraint from GOTO survey photometry.

Fig. 1. GOTO discovery triplet of GOTO0650 as seen by citizen scientists on the Kilonova Seekers project, with the science frame, the historical reference image, and the difference image. The inner box corresponds to a scale of ≈ 80 arcsec across. The labelling indicates the time of observation of this source and the GOTO site and survey mode that the observation was taken from. Below the science image, we show a series of subframes of the four individual exposures that were stacked to create the science image.

scope and Rapid Response System (Pan-STARRS) DR1 imaging (Chambers et al. 2016). Without the Kilonova Seekers volunteers flagging this object, rapid follow-up would not have been possible, and this object may have been missed entirely. Citizen science is a powerful method for driving discoveries in vast datasets that must be sifted in a focused way by scientists, which leaves ample room for novel serendipitous discoveries. The discovery image of GOTO0650 is presented in Figure 1, as seen by the volunteers. A clear underlying blue source is located at this position in Legacy Surveys (Dey et al. 2019) and Pan-STARRS 4π (Chambers et al. 2016) Survey imaging, which we identified as GOTO0650 in quiescence. The source has magnitudes $g = 21.84$, $r = 21.68$, and $z = 22.02$ in the Legacy Surveys DR10, with ($g - r \approx 0.2$). Taken with the GOTO discovery magnitude, this implies an outburst of ≈ 8.5 mag in amplitude.

We inspected available forced photometry (photometric observations extracted at the known position) of GOTO0650 in quiescence from GOTO, the Asteroid Terrestrial-impact Last Alert System (ATLAS; Tonry et al. 2018), ASAS-SN, and the Zwicky Transient Facility (Bellm et al. 2019) via the GOTO Lightcurve Service (Jarvis et al., in prep.), ATLAS Forced Photometry Server (Shingles et al. 2021), ASAS-SN Sky Patrol (Kochanek et al. 2017), and ZTF Forced Photometry Service (Masci et al. 2023). We found no evidence for prior outbursts during the covered time span (approximately 4 years). We engaged in a more comprehensive search for historical outbursts using plate archives, and we discuss a candidate outburst in 1951 in more detail in Section 3.

Follow-up spectroscopy with the Nordic Optical Telescope (NOT) and Liverpool Telescope (LT; Steele et al. 2004) obtained ≈ 4 days post discovery confirmed the Galactic nature of this source (Killestein et al. 2024c), which showed a blue continuum with Balmer absorption lines at $z = 0$, weak He I $\lambda 4471$, and weak Na ID absorption. The spectrum showed no emission lines at the time of classification, which is consistent with observations of the WZ Sge system GW Lib at maximum light (Hiroi et al. 2009). Because of the changing nature of the spectrum of GW Lib (and other systems) over its outburst, we triggered an intensive observing campaign to investigate the nature of the accretion disc during the outburst.

Table 1. Summary of all photometric data of GOTO0650.

Facility	Bands	Number of images
GOTO	*L*	52
LCO 0.4 m	*ugriz*	326
Swift	*UVW1,UVM2,UVW2,U*	12
TTT	*ugriz*	78
pt5m	*BVRI*	72
LJT	*CV*	1

3. Observations and data reduction

This section presents the detailed photometric and spectroscopic observations for GOTO0650 along with the data reduction process. Upon discovery, we promptly initiated an intensive follow-up campaign using multiple facilities. The first follow-up photometry of GOTO0650 was captured just 30 minutes after the Kilonova Seekers platform issued the alert, and the first spectrum was obtained within 4 days.

3.1. Photometry

Upon discovery, we quickly began an intensive photometric follow-up campaign of GOTO0650 using a number of facilities (summarised in Table 1).

We obtained a sequence of *ugriz* photometry with the 0.4 m robotic telescopes of the Las Cumbres Observatory Global Telescope Network (LCOGT; Brown et al. 2013) through the Kilonova Seekers – LCO: STAR (Surveying Transients with Amateur Researchers) program[2], an LCO Global Sky Partner. The Kilonova Seekers – LCO: STAR educational program was specifically designed as an extension of the GOTO Kilonova Seekers citizen science project to enable volunteers to be involved in all aspects of transient astronomy: from the discovery, to triggering further observations, to classification; learning how to reduce data, and how to make and analyse light curves and colour images with guidance and support from the Kilonova Seekers team. A mixture of high-cadence observations and staged follow-up were performed. Initial observations consisted of a continuous sequence of 30 s exposures for a 30-minute window in *g* band to identify any short-term variability, with daily follow-up in *ugriz* bands to characterise the decline of the light curve. The data reduction was performed with the BANZAI pipeline (McCully et al. 2018).

Nightly observations were obtained with the pt5m 0.5m telescope (Hardy et al. 2015) at Roque de los Muchachos, La Palma. Observations were obtained with *BVRI* filters, and they were calibrated and stacked with custom pipelines.

Observations were also obtained with the 80 cm TTT1 telescope, which is part of the Two-meter Twin Telescopes[3] project, in the *ugriz* filters with a iKon-L 936 CCD. The data were calibrated with a custom pipeline. Observations were also obtained on 2024 December 3 using the Lijiang 2.4 m Telescope (LJT) with a 2 min exposure in the clear (*CV*) band. The LJT data were calibrated to *V* band using source colour information estimated from LCO and TTT data.

Photometry on all reduced frames was performed with a custom photutils-based (Bradley et al. 2016) seeing-matched

aperture photometry pipeline (Killestein et al., in prep.) to ensure that all photometry was performed in a standardised way. All *griz* photometry was calibrated to Pan-STARRS-1 (Chambers et al. 2016) field stars, while *u*-band photometry was calibrated to synthetic photometry derived from the Gaia DR3 BP-RP spectra of stars in the field (Gaia Collaboration 2023). Johnson-Cousins *BVRI* photometry was approximately calibrated to Pan-STARRS using synthetic magnitudes for field stars derived using the transformations by Tonry et al. (2012). All photometry was corrected for a foreground reddening of E_{B-V} = 0.056 using the 3D reddening maps of Lallement et al. (2022), Vergely et al. (2022), evaluated at the inferred distance of GOTO0650 (see Section 4), assuming a Fitzpatrick (1999) extinction curve when adjusting our spectra. We kept this reddening estimate fixed throughout, but propagated uncertainty arising from the distance forwards in parameter estimates. The magnitudes are given in their natural systems (AB for *ugriz*, and Vega for *BVRI*). The collated photometry of GOTO0650 is presented in Figure 3 and is summarised in Table A.1.

We also included all available photometry from GOTO survey observations in our light curve. The GOTO images were processed with the kadmilos pipeline (Lyman et al., in prep.), and forced photometry at the location of GOTO0650 was performed using the GOTO Lightcurve service (Jarvis et al., in prep.).

We obtained two epochs (2024 October 19 and 2024 October 20) of high-cadence photometry with Gotito, the GOTO CMOS Pathfinder instrument located next to the GOTO-N node (see Godson et al., in prep.). Observations were predominantly taken in the *L*-band filter at a cadence of 30 s using a Sony IMX411 CMOS sensor. Low-level image calibration was performed with custom pipelines. For inclusion on light curve plots and tables, we calibrated the Gotito to *g* band by accounting for the colour term using the observed *g − r* colour derived from LCO observations close in time.

Photometry from a number of citizen scientist observers was retrieved via the American Association of Variable Star Observers (AAVSO) International Database[4] in the Johnson-Cousins (*BVR*) and *CV* bands, but only *V* and *CV* observations are included in this work. To remove offsets and standardise these data, we computed per-observer offsets based on overlapping intervals of LCO and TTT *gri* data (transformed to Johnson *V* with the relations of Tonry et al. 2012). We included only observations in this standardisation process where $V <$ 17 mag to ensure robust corrections. We interpolated this reference light curve to each observer's individual photometric epochs with a thin plate spline[5] and computed the (σ-clipped) median deviation across the observers' photometry as the offset. The per-observer shifts, with a few exceptions, are small, typically <0.1 mag. Nevertheless, it is crucial to correct for them to ensure smooth light curves in the poorly sampled regions in our multi-colour photometry, such as the dip phases, where the intrinsic scatter is higher.

Furthermore, we searched for evidence of historical outbursts using the light curve tool provided by the Digital Access to a Sky Century at Harvard (DASCH) project (Grindlay et al. 2012). A single source was recovered at a distance of 13″ from the position of GOTO0650 with a detection on 1951 February 26 (MJD 33 703.06) at an apparent magnitude of 13.0 (Plate ac41904) with a non-detection 20 days prior (Plate rh15570). We show cutouts of these plates in Figure 2. Whilst this initial separation between our measured position of GOTO0650
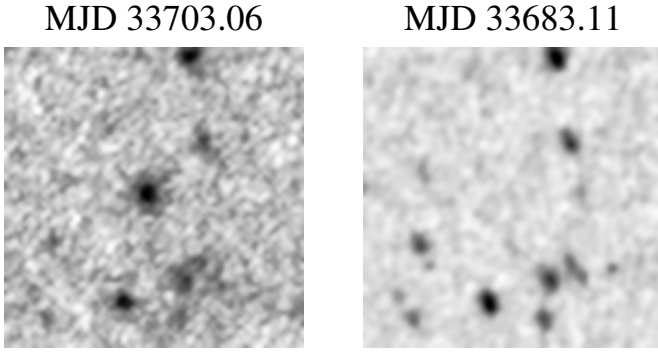

MJD 33703.06   MJD 33683.11

Fig. 2. Harvard photographic plates retrieved via DASCH depicting a historical GOTO0650 superoutburst on MJD 33 703.06 (1951.15) after correcting the alignment for additional distortion. We also show an image taken on MJD 33 683.11 (1951.037).

and this putative historical superoutburst is large (considering the plate scale of $4'' \, \text{pix}^{-1}$), there is some evidence for unaccounted-for distortions in the plate local to GOTO0650. Recomputing the astrometry with a smaller cut-out of the plate (via `astrometry.net`; Lang et al. 2010) yielded a better concordance (≈ 2 pixels). We therefore took this source detection to be an outburst from GOTO0650, and we elaborate further on the implications of this historical superoutburst in Section 5.

3.2. Spectroscopy

We obtained a number of spectra with the Alhambra Faint Object Spectrograph (ALFOSC) mounted on the NOT at Roque de los Muchachos Observatory, La Palma. Specifically, grisms number 4, 7, and 17 were used. These spectra were reduced with the PyNOT[6] pipeline. Further spectra were obtained with the SPectrograph for the Rapid Acquisition of Transients (SPRAT; Piascik et al. 2014) on the LT (Steele et al. 2004), and they were reduced with Pypeit (Prochaska et al. 2020). Spectra were also obtained with an ALPY spectrograph using the 200 and 600 lines per mm grisms (45 and 12 Å resolution respectively) mounted on a 0.28 m telescope at Three Hills Observatory. The spectra were reduced using ISIS[7] and calibrated in relative flux using reference stars at matching airmass. These spectra were retrieved via the BAA Spectroscopy Database[8]. All spectra were rescaled with a polynomial correction factor to match contemporaneous photometry to ensure that any subtle changes in the continuum shape were robust and to ensure a good absolute flux calibration. The full details of all spectroscopic observations included in the paper are tabulated in Table 2.

3.3. X-ray and UV observations

Observations were made using the Follow-up X-ray Telescope (FXT) on the Einstein Probe (Yuan et al. 2022) spacecraft. The FXT has a passband between 0.5–10 keV and a spatial resolution of 20–24″ (half-power diameter) on axis. The first of seven observations was made 2.48 d after the discovery, and the most recent was made 34.67 d after discovery. A significant if weak X-ray source was detected at a position consistent with the optical position.

Observations of GOTO0650 were also made by the Neil Gehrels Swift satellite, with seven epochs in total (PIs: Ramsay, Bhattacharaya, Chandra). The start time was 3.9–34.1 d after discovery. The observations using the X-ray Telescope (XRT) were generally short (<1 ks), and thus, no X-ray source was detected at the position of GOTO0650 during any of the pointings.

Simultaneous UV observations with the Ultra-Violet Optical Telescope (UVOT) (Roming et al. 2005) detected GOTO0650 in all pointings. Observations were scheduled in filter of the day mode, with GOTO0650 being observed in the $UVW2$, $UVM2$, $UVW1$, and U bands. Because GOTO0650 is a point source and was concretely detected in all pointings, we used the standard UVOT source catalogues. The UV flux of GOTO0650 broadly traces the optical evolution, as expected. We elaborate further on the detailed evolution below.

4. Analysis and results

4.1. Photometric evolution

The photometric series of GOTO0650 is comprehensive, with a dense coverage through the first two months of the light curve evolution. In Figure 3, we present the photometric evolution of GOTO0650 from our intensive monitoring, from curated survey data, and from AAVSO observers. We focus on a number of key phases in the light curve of this object: On the initial discovery, on the decline from the peak phase, on an early dip, and then on a deeper decline into the pre-quiescent phase with repeated strong outbursts.

The initial superoutburst of GOTO0650 was detected in an image from the GOTO all-sky survey obtained on 2024 October 4 03:36:36 at $L = 13.36$ mag, not corrected for extinction. The exact outburst date is constrained by a prior GOTO observation (2024 October 2 03:36:32), which reached a 5σ limiting magnitude of $L = 20.14$. This implies a rise rate of $\gtrsim 3.4 \, \text{mag d}^{-1}$. In the absence of any more constraining non-detections, we took the time of outburst to be MJD $60,586.2 \pm 1.0$, which is the midpoint of the first detection and of the last non-detection. The uncertainty is half the span. The true outburst date likely lies in the second half of this interval, based on rise rates (≈ 7 mag/day) from uninterrupted coverage of other WZ Sge-like systems with Kepler (e.g. Ridden-Harper et al. 2019). At peak, the V-band apparent magnitude of the light curve is $m_V = 13.04 \pm 0.05$, corrected for foreground extinction as noted in Section 3. We estimated the distance to GOTO0650 by using $M_V = 4.5 \pm 0.3$ derived from the peak absolute magnitudes of known WZ Sge systems (Patterson 2011). Taking the peak $V = 13.04$ inferred above, we determined a distance of 510^{+80}_{-60} pc.

Over the next 14 days, GOTO0650 showed a steady decline of $\approx 0.1 \, \text{mag d}^{-1}$ in all bands, estimated via linear regression. The colour (see Figure 4) over this time also showed a marginal evolution. It reddened in the $g - r$ and $g - i$ colour indices by ≈ 0.1 mag. Figure 5 shows the overall co-evolution of the colour indices with respect to the outburst phase. Spectroscopy during this phase showed a blue continuum with strong Balmer absorption (discussed in greater detail in Section 4.4). This indicates that the emission is dominated by a geometrically thick disc.

At +14 d post discovery, GOTO0650 entered a short and shallow dip in brightness, similar to those seen in WZ Sge systems (Kato 2015). A zoom-in is depicted in Figure 6. The depth was ≈ 1.5 mag in V and R band and lasted for only 4 days. The profile of the dip was slightly skewed and had a slower drop in ($t_{1/2} = 0.58$ d) and more rapid rise out

Table 2. Log of spectra obtained of GOTO0650 during our observing campaign.

Instrument	Grism	Date (UT)	Phase (d)	Exp. time (s)	Airmass	Slit width (arcsec)	R	Range (Å)
NOT ALFOSC	4	2024 Oct 08 05:00:30	4.1	120	1.24	1.0	360	3200–9600
LT SPRAT	Blue	2024 Oct 08 05:25:57	4.1	200	1.21	1.8	350	4020–8100
THO ALPY200		2024 Oct 11 00:50:32	6.9	1201	1.27	3.1	166	3750–7500
LT SPRAT	Blue	2024 Oct 12 04:30:55	8.0	240	1.26	1.8	350	4020–8100
THO ALPY200		2024 Oct 13 02:01:40	8.9	3005	1.14	3.1	166	3750–7500
THO ALPY200		2024 Oct 15 00:26:12	10.9	3606	1.29	3.1	166	3750–7500
LT SPRAT	Blue	2024 Oct 17 03:26:06	13.0	300	1.36	1.8	350	4020–8100
NOT ALFOSC	7	2024 Oct 20 02:38:31	16.0	300	1.47	1.0	650	3650–7110
LT SPRAT	Blue	2024 Oct 24 03:51:48	20.0	300	1.25	1.8	350	4020–8100
THO ALPY600		2024 Oct 27 00:41:45	22.9	7215	1.18	3.1	518	3750–7500
NOT ALFOSC	7	2024 Nov 01 05:49:44	28.1	3600	1.16	1.0	650	3650–7110
NOT ALFOSC	7	2024 Nov 10 01:38:17	36.9	1800	1.43	1.0	650	3650–7110
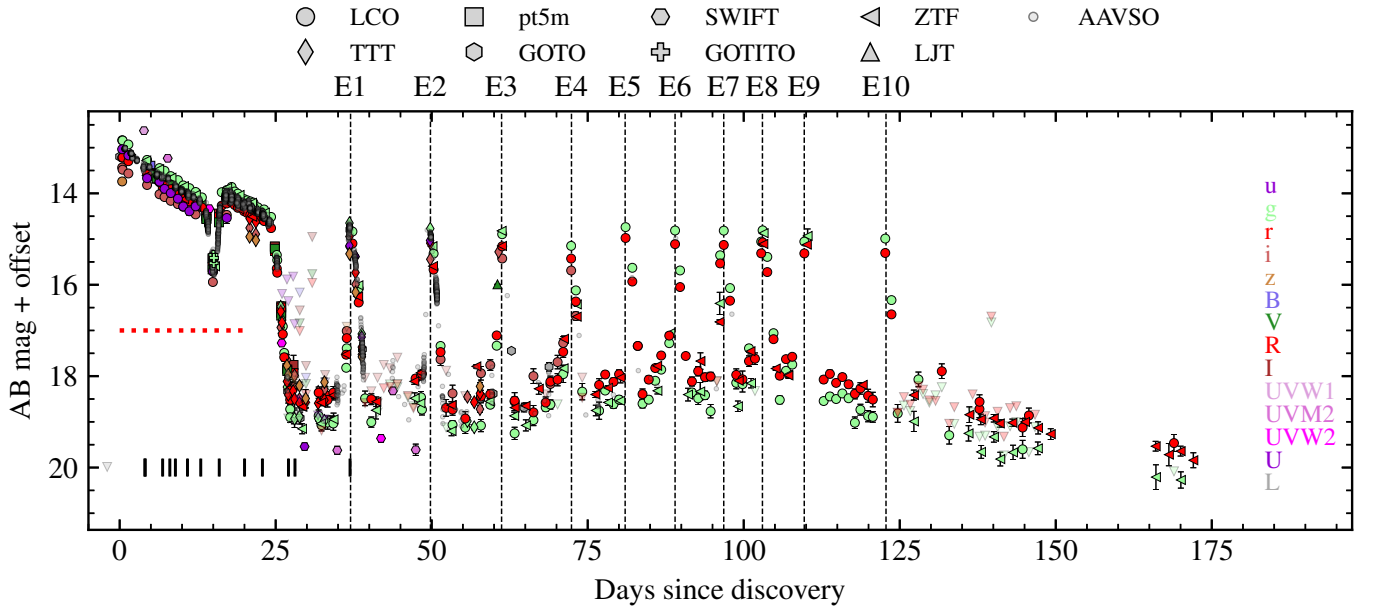
Fig. 3. Collated photometry of GOTO0650 (see Table 1), shown relative to the GOTO discovery epoch. An overview of this photometry and the associated uncertainties is presented in Table A.1. The error bars are typically too small to be seen. The photometry was corrected for Galactic extinction. The vertical markers indicate phases in which the spectra were obtained. Non-detections are overplotted with the triangular markers where available, corresponding to 5σ upper limits, with the opacity facilitating visualisation in areas of dense coverage. The vertical lines annotated E_N correspond to the Nth echo outburst observed, and the dotted red line indicates the magnitude at which we distinguish between high and low states.

($t_{1/2} = 0.87$ d). The dip was essentially achromatic and showed no significant change in the colour indices, as evident from the photometry we obtained at the bottom of the dip. Approximately around this time ($+13.8$ d; see Section 4.3), ordinary superhumps emerged with a characteristic asymmetric profile. They contributed to the excess scatter in the lower-cadence light curve. This is consistent with the timing of the ignition of superhumps in EG Cnc (Patterson et al. 1998), whose light curve is very similar to that of GOTO0650. After the conclusion of this short-lived event, GOTO0650 rose to ≈ 0.1 mag brighter than on the previous plateau, before it declined at a very similar rate.

The main dimming event in GOTO0650 began $+25$ d post discovery, dropping from $g = 15$ mag into a persistent low state of about $g = 19$ mag. The decline was rapid, at ≈ 1.5 mag d^{-1} in

V band. The transition to the low state showed a stark shift in colour that transitioned from $g - r \approx -0.3$ to $g - r \approx 0.5$ mag, with a similar evolution mirrored in $r - i$ (Figure 5).

4.2. Echo outbursts

Approximately 36.5 days after the initial superoutburst, GOTO0650 entered a phase that was punctuated by a number of 'echo outbursts', which are short-duration rebrightenings that were observed in a relatively small number of CVs (e.g. Patterson et al. 1998; Kato et al. 2004). GOTO0650 has shown ten rebrightenings, E1–10 hereafter, which almost reached the pre-dip brightness (typically with an amplitude of ≈ 3.7 mag), and appeared to be blue in colour. The sampling of the photometry covering echo bursts E3–10 is lower than during E1–2, but
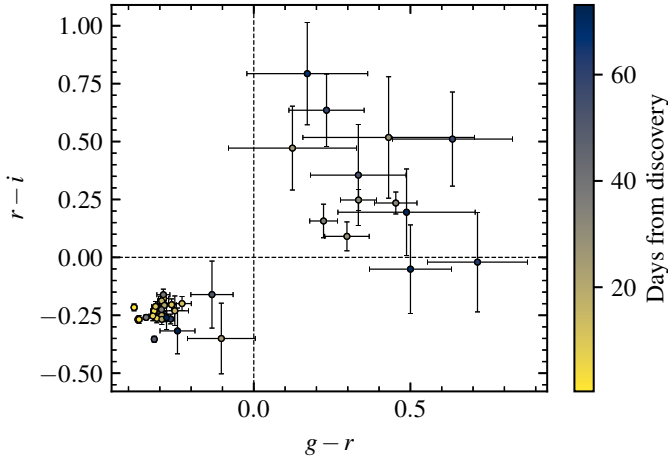
Fig. 4. Colour locus plot of GOTO0650 from LCO and TTT *gri* photometry, showing the distinct two clusters corresponding to the high and low state. The points are shaded to show the phase relative to discovery.
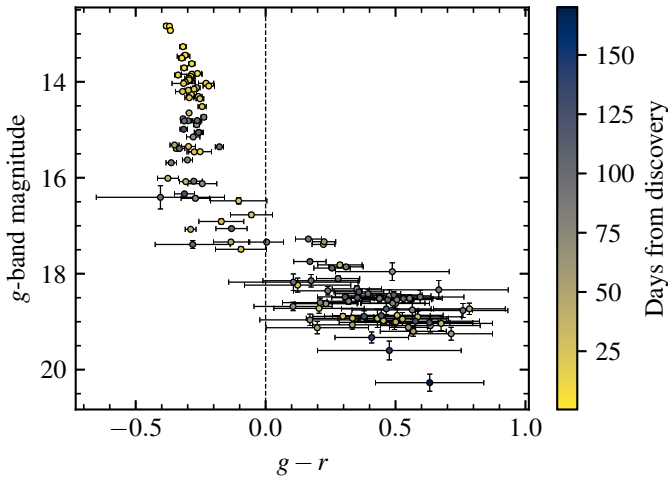
Fig. 5. *g* − *r* colour of GOTO0650 as a function of apparent magnitude. The colour scale shows the phase relative to discovery. A clear change in the source colour with magnitude is visible and shows a strong reddening on the way to the low state.

there is some indication that the durations of bursts E3–10 are shorter than those of bursts E1–2.

We note the time of the echo outbursts and the time since the previous outburst in Table 3 and Figure 7. Between E2 and E9, the recurrence time decreased from 13.5 d to 6.5 d, with an increase between E10 and E9 of 16.0 d. The mean recurrence time was 8.7 d and 7.9 d when we exclude E10. This follows the same trends as EG Cnc, which showed six echo outbursts in its 1996 outburst with a mean recurrence time of 7.1 d (Patterson et al. 1998). The mean time between the echo outbursts in GOTO0650 is longer than for most WZ Sge systems, as reported by Kato (2015) and Meyer & Meyer-Hofmeister (2015), where they are generally 3–5 d. No colour change in *g* − *r* accompanies this change in the outburst state. Although the sampling precludes a definitive statement, there is a hint that the brightness level between outbursts increased as the outburst proceeded (see Meyer & Meyer-Hofmeister 2015).

No further echo outbursts were observed beyond E10 on day 125, with confident detections from both our LCO photometry and the ZTF over this time period. Our latest observations,

Table 3. Time of the echo outbursts (see Figure 3) since the discovery date and the time delay since the previous echo outburst.

Burst number	Time since outburst (d)	Time since previous burst (d)
E1	36.5	–
E2	50.0	13.5
E3	61.0	9.0
E4	72.5	11.5
E5	81.0	8.5
E6	89.0	8.0
E7	96.0	7.0
E8	103.0	7.0
E9	109.5	6.5
E10	125.5	16.0

around 160 days post discovery, showed that GOTO0650 continued to decline slowly in brightness and returned to quiescence. This likely indicates that this was the conclusion of this super-outburst of GOTO0650.
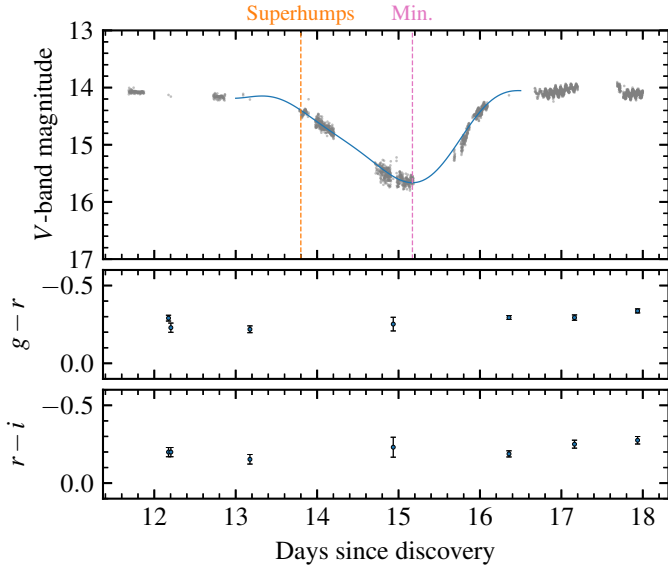
4.3. Short-timescale variability

Throughout the evolution of GOTO0650, high-cadence photometry was obtained from both citizen scientists and professional observatories. This photometry was initially devoid of obvious variability for about the first two weeks of evolution, without evidence for superhumps during this time frame at the precision of the available data, which come primarily from AAVSO observers. The first credible detection of ordinary superhumps was seen in the observations of Vanmunster (reported in `vsnet-alert 28024`)[9] on 2024 October 18, approximately 13.8 days post discovery. The onset of superhumps is neatly illustrated in Figure 6, where the epoch of the onset is shown with the dashed orange line. This length of delay in the appearance places it on the longer side of the distribution shown by WZ Sge systems (see Fig. 18 of Kato 2015) and coincides with the beginning of the first dip discussed in the previous section. The uncertainties on the superhump parameters at this first epoch are large because approximately one cycle was observed. We therefore did not include this epoch in any analysis.
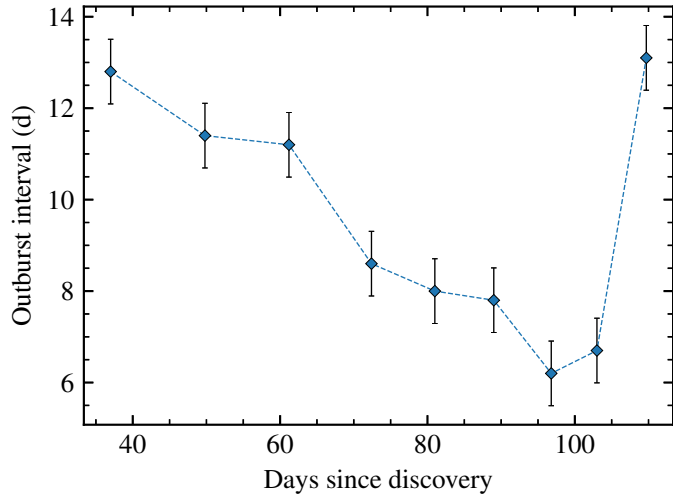
To investigate the emergence of superhumps and the evolution of the period, we inspected and computed Lomb-Scargle (Lomb 1976; Scargle 1982) periodograms of the individual high-cadence time-series observations in *V*, *CV*, and *g* bands. The photometry was detrended with a linear fit to remove longer-timescale evolution. Figure 8 illustrates the superhump period and superhump amplitude as a function of time post discovery to probe their evolution. Approximate polynomial fits (linear in the superhump period and cubic in the superhump amplitude) are overplotted to guide the eye. The uncertainties on the best-fitting period were derived from the full width half maximum (FWHM) of the periodogram peak. This is a purely statistical error and does not fold in potential systematic uncertainties. The super-hump amplitude was estimated as the peak-to-peak amplitude of the best-fitting sinusoid, and the uncertainties were conservatively estimated from the standard error of the residuals. We also phase-fold the AAVSO light curves around the time of maximum

---

[9] http://ooruri.kusastro.kyoto-u.ac.jp/mailman3/hyperkitty/list/vsnet-alert@ooruri.kusastro.kyoto-u.ac.jp/message/WZ7VAQUUGELF22D54Q3YXVGLXN7QTN6Q/
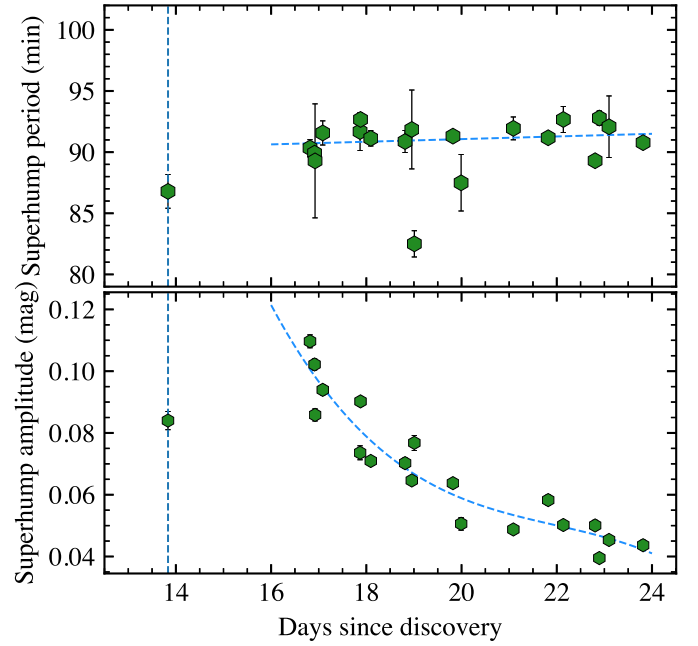
Fig. 6. High-cadence *V*-band photometry around the dip observed in GOTO0650 from AAVSO, LCO, pt5m, and TTT. The blue curve shows a spline interpolation of the data. The vertical dashed line shows the initial onset of superhumps as the dip began. The $g - r$ and $r - i$ colour indices show no significant evolution through the dip. The dip shows a marked asymmetry, with a slow ingress and rapid egress. High-amplitude superhumps with an amplitude of ≈ 0.1 mag are visible immediately after the dip.

Fig. 8. Superhump period and amplitude evolution in GOTO0650. The time is given relative to the GOTO discovery date. The dashed blue line indicates the first epoch at which superhumps were detected. The error bars in both plots are the 1σ statistical uncertainties. An illustrative fit to the superhump period and amplitude is overplotted to show the overall evolution.
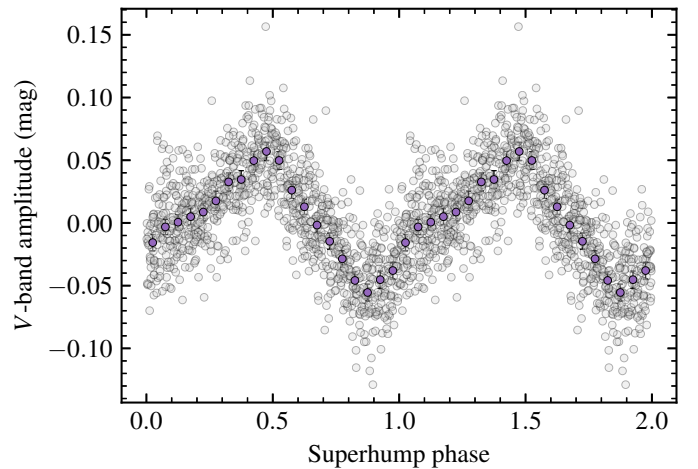

Fig. 7. Inter-burst timescale for the echo outbursts observed in GOTO0650. The error bars correspond to the half-width of a typical outburst. GOTO0650 shows a marked evolution towards more frequent echo outbursts.

Fig. 9. Phase-averaged light curves from AAVSO observers between days 16 and 18 that reveal the profile of the observed superhumps close to their maximum amplitude. The phase is given arbitrarily relative to discovery date because measure of when the superhumps first emerged is not precise.

superhump amplitude (days 16–18) and combined them together in phase bins of 0.05 to better reveal the superhump profile from the scattered data. The points in each phase bin were combined with the inverse-variance weighted mean, and they are plotted in Figure 9. The profile has a clear asymmetry.

The superhump period was approximately 91 ± 1 min around 17 d post discovery and remained broadly consistent with this throughout. It showed some marginal evolution to longer periods. Because of the uncertainties in the period estimation, it is not trivial to robustly estimate the period derivative $\dot{P}$. Based on the revised stellar evolutionary models of Knigge et al. (2011),

the mass ratio, $q = M_1/M_2$, is 0.05 or 0.12 depending on whether it is a post- or pre-minimum binary. Assuming that the superhumps arise due to a tidal instability at a radius at the 3:1 resonance with the secondary, we used the relation given by Equation (8) of Kato & Osaki (2013), which is appropriate to the mean of stage B superhumps. With this, we determined an orbital period of 90.4 or 88.5 min (post- and pre-period minimum respectively) with typical statistical uncertainties of 1 min. The superhump amplitude showed a strong evolution and reached a maximum around +16 d post discovery of 0.1 mag peak to peak,
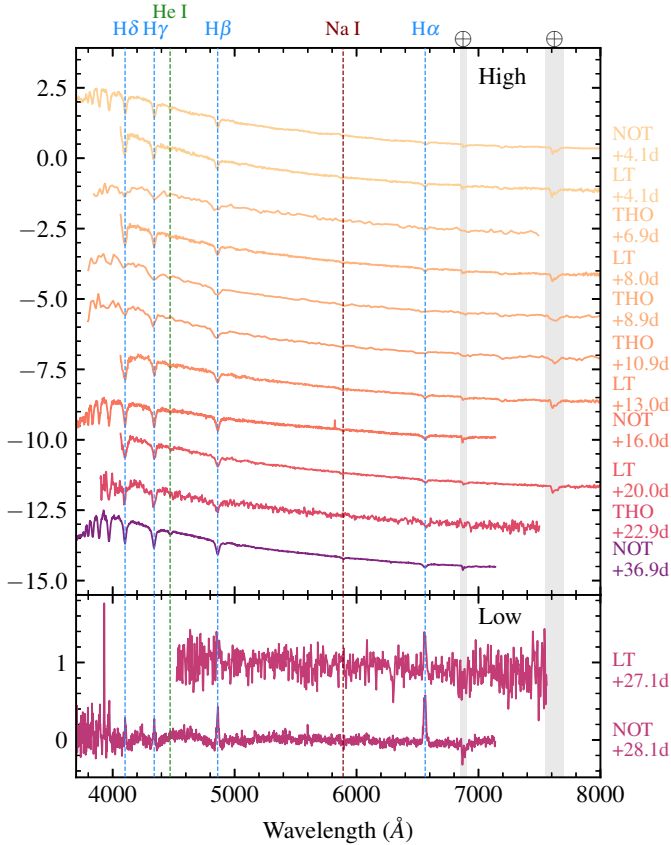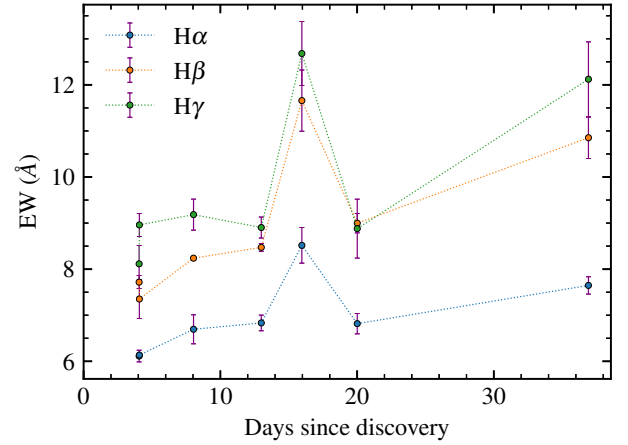
Fig. 10. Spectra of GOTO0650 split into high and low state for visualisation purposes. All spectra were flux-calibrated to contemporaneous photometry and corrected for Galactic extinction. The key spectral features are indicated by dashed lines, and the telescope and epoch of each observation are displayed.

Fig. 11. Equivalent widths and uncertainties for the most prominent absorption features in the high state for GOTO0650. The uncertainties were estimated via Monte Carlo resampling of the spectra. The EWs increase over time overall, with a marked jump around the time of the first dip.

roughly after the first dip concluded. It then declined rapidly after this phase before it became largely undetectable beyond 24 days. Observations of the 2021 outburst of V627 Peg showed that prior to the first decline phase, the amplitude of the superhumps was only ~0.05 mag (Tampo et al. 2023), which is less than we observed in GOTO0650. A more detailed characterisation of the superhumps, in particular, $O - C$ diagrams and similar analyses requiring precise phasing, is deferred to a follow-up paper.

4.4. Spectral evolution

The spectral evolution of GOTO0650 is shown in Figure 10. Because of the clear differences between the two states, we split the spectra into 'high' and 'low' states for the further analysis. In both states, we computed line parameters (equivalent width, flux, and FWHM), which we tabulate in Table 4.

The spectra in the high state show a predominantly blue continuum with strong Balmer absorption features. Hα appears to be strongly suppressed compared to the other Balmer lines. This is expected when the accretion disc is optically thick, as reported by Tovmassian et al. (2022), who showed spectra of the WZ Sge system V455 And over its 2007 superoutburst. The spectrum also shows weak He and Na absorption lines, but they are only well detected in high-quality spectra. Our higher-resolution NOT spectra (grism 7, $R \approx 650$) at +16 d shows no evidence of weak emission in the line cores.

The absorption features show some evolution in the equivalent width through the outburst phase, which matches the overall light curve evolution well, with the lines deepening as the continuum drops away. The equivalent width of all lines clearly decreases around +15 d, corresponding to the initial dip, followed by a drop as the overall luminosity increases (see Fig. 11).

We obtained observations in the low state on days 27 and 28 with LT SPRAT and NOT ALFOSC, respectively. Despite the poor signal-to-noise ratio of the SPRAT spectrum, Hα is clearly detected in emission. The NOT ALFOSC spectrum on the next day shows a wealth of spectral features: narrow Balmer emission lines clearly detected up to H10, very weak He IIλ4686 and Fe IIλ5168, strong Ca II H&K emission, and some broad absorptions superimposed on a flat continuum. The line widths of the emission features are $\approx$1000 km s^{-1} and are only marginally resolved in our spectrum. This spectrum is depicted in Figure 12, alongside a WD spectrum that approximately matches GOTO0650 in quiescence. This spectrum is rescaled by a factor of 10 to enhance visibility.

In contrast to WZ Sge and V455 And (e.g. Gilliland et al. 1986; Tovmassian et al. 2022), where complex He Iλ5876,6676 features are present, the spectrum of GOTO0650 lacks these features at a level that would be easily detected in our NOT ALFOSC spectrum. Other WZ Sge systems such as V386 Ser (e.g. Inight et al. 2023) lack strong He I and He II emission, however. Clear indications of a double-peaked emission profile in Hα arise from the accretion disc, although it is not well resolved. This may be due to the low spectral resolution ($R \approx 650$), or alternatively, it may suggest a low binary inclination (Horne & Marsh 1986). All Balmer lines show a pronounced asymmetry between the red and blue peaks, with a slightly enhanced red component. Although it is difficult to measure the precise separation between the two maxima, the velocity separation of the two profile maxima in Hα is $\approx$370 km s^{-1}. The ratios of EWs of Hα:Hβ:Hγ in the low state are 2.2:1.4:1, and the equivalent widths themselves are broadly lower than those of typical cataclysmic variables in quiescence (e.g. Szkody et al. 2004).

Some limited spectroscopy was obtained during the echo outburst phases, but was largely hampered owing to their short timescale. The spectrum obtained on day 36, at the peak of the

Table 4. Line parameters (equivalent width, FWHM, and line flux) of various key spectral features seen in the optical spectra of GOTO0650 throughout its evolution.

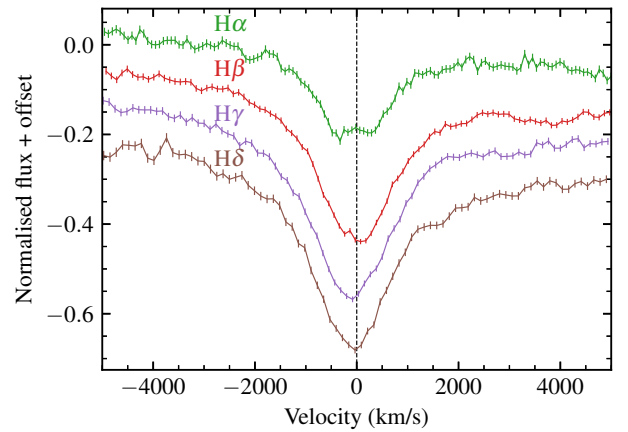| Phase (d)	Hα			Hβ			Hγ		
	EW (Å)	FWHM (km/s)	$F_{H\alpha}/10^{-15}$ (erg/cm²/s)	EW (Å)	FWHM (km/s)	$F_{H\beta}/10^{-15}$ (erg/cm²/s)	EW (Å)	FWHM (km/s)	$F_{H\gamma}/10^{-15}$ (erg/cm²/s)
4.1	6.1 ± 0.2	1880	–	7.7 ± 0.2	1900	–	8.1 ± 0.2	1920	–
4.1	6.1 ± 0.3	1750	–	7.3 ± 0.3	1810	–	9.0 ± 0.3	2040	–
8.0	6.7 ± 0.3	1460	–	8.2 ± 0.2	2050	–	9.2 ± 0.3	2120	–
13.0	6.8 ± 0.4	1720	–	8.5 ± 0.3	2170	–	8.9 ± 0.4	2070	–
16.0	8.5 ± 0.3	1720	–	11.7 ± 0.2	1870	–	12.7 ± 0.3	2000	–
20.0	6.8 ± 0.4	1650	–	9.0 ± 0.3	2180	–	8.9 ± 0.4	2000	–
28.1	−13.6 ± 0.6	1010	1.9 ± 0.1	−9.0 ± 0.6	1000	1.3 ± 0.7	−6.5 ± 0.7	760	0.9 ± 0.1
36.9	7.6 ± 0.1	1730	–	10.9 ± 0.1	1930	–	12.1 ± 0.1	2080	–

Notes. Uncertainties correspond to 1σ confidence intervals as estimated via Monte Carlo resampling. The line fluxes are only given for emission lines, and we preserved the sign of EW to flag emission and absorption.
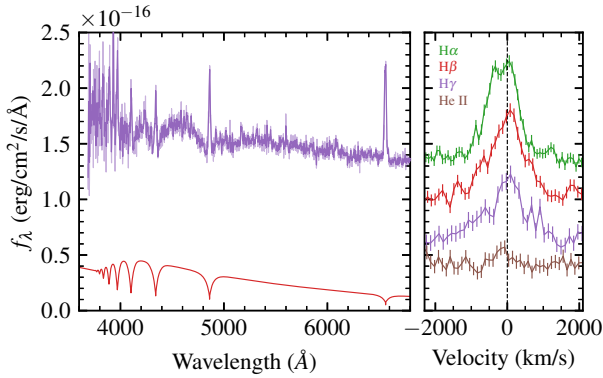
Fig. 12. NOT ALFOSC gr7 spectrum of GOTO0650 obtained at +28.1 d at the bottom of the decline off plateau ($g \approx 19$). A five-pixel variance-weighted boxcar filter was applied to reduce noise. The inset panel is centred on the prominent Hα emission line, showing tentative indications of a more complex profile, but ultimately limited by spectral resolution. The WD contribution was estimated from the best-fitting model SED estimated in Section 4.5, scaled to the distance inferred in Section 4 assuming a fixed $\log g$ of 8 and a radius inferred from the sequences of Bédard et al. (2020).

Fig. 13. Balmer lines as observed in the +36 d spectrum obtained at the peak of the first echo outburst. There are clear differences between the line profiles moving to higher ionisation lines, and the varying line profiles are well explained by the differences in amplitude between the Balmer emission seen in the low-state spectrum obtained on 28 d.

first echo outburst, shows a Hα profile with a double dip where the line core appears to be filled in by emission, and more typical profiles are seen in the other lines. Figure 13 illustrates these line profiles, normalised to the continuum.

Further spectroscopy deeper into quiescence is required to constrain system parameters such as the orbital period P and the binary mass ratio q, which are challenging to constrain robustly with the dataset presented here.

### 4.5. Spectral energy distribution in quiescence

There is some limited archival photometry of GOTO0650 in the quiescent state in the Pan-STARRS (Chambers et al. 2016; *grizy* bands) and Legacy Survey (Dey et al. 2019; *grz* bands). Although we lack detections in bands bluer than g (most notably, we lack near-UV photometry to tightly constrain the temperature and near-IR to better know the nature of the donor star) there is still some utility in modelling the SED to attempt to infer parameters of the system. This is useful to consider the evolutionary implications for the WD in the GOTO0650 system.

Under the assumed distance modulus of $\mu = 8.3 \pm 0.2$ derived from the absolute peak magnitude of WZ Sge systems (Patterson 2011), GOTO0650 has a V-band absolute magnitude in quiescence of $M_V = 13.1 \pm 0.2$, which is compatible with absolute magnitudes for WDs and the donor stars in these types of systems. Because of the blue observed colour, it is a safe assumption that the majority of this flux arises from the WD in the system. We proceeded under this assumption and found no strong excess in the redder bands or donor spectral features, but we note that GOTO0650 is not formally detected in the y band. No astrometric solution for GOTO0650 is available from Gaia as of the current data releases. A more detailed characterisation of the system is therefore challenging in absence of a parallax. To constrain the properties of the WD in GOTO0650, we inferred the temperature and surface gravity using the Pan-STARRS observed colours in conjunction with synthetic photometry derived from the Bergeron[10] model grids (Holberg & Bergeron 2006; Tremblay et al. 2011) and the Bédard et al. (2020) evolutionary sequences assuming a thick H envelope. Evolutionary

---

[10] https://www.astro.umontreal.ca/~bergeron/CoolingModels/
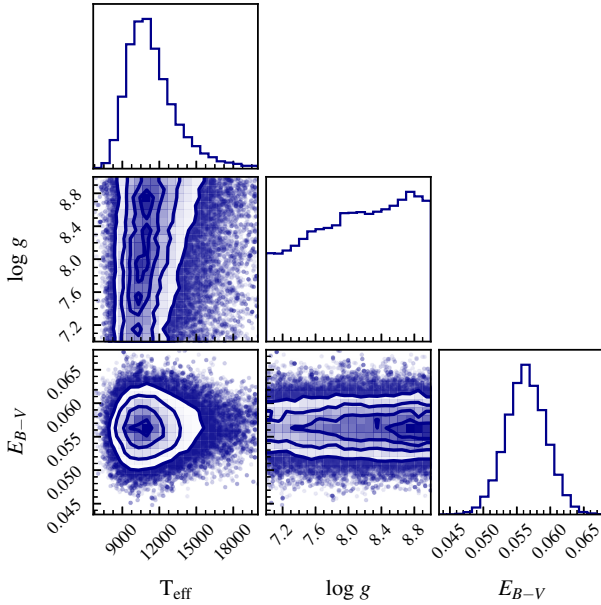
Fig. 14. Posterior distributions from modelling the available Pan-STARRS photometry of GOTO0650 in quiescence. The reddening parameter is essentially prior dominated, but a reasonable constraint on effective temperature is obtained.

sequences were interpolated using the `MR_relation`[11] Python code. Because of the poorly constrained distance that was derived from the empirical Patterson 2011 relation and not from a geometric parallax, we only used colour information in our fitting. We only considered the available Pan-STARRS photometry in this analysis to avoid any potential systematic errors associated with mixing survey magnitude systems. We assumed a prior uniform over the whole $T_{\rm eff}$-$\log g$ grid and assumed a fixed reddening value, but we propagated the uncertainties (primarily stemming from distance estimate) to avoid underestimating the uncertainties in the WD parameters. We assumed that the observed colours $g - r$, $r - i$, $i - z$, and $z - y$ can be modelled with a product-Gaussian likelihood, and we sampled the posterior distribution using the `emcee` (Foreman-Mackey et al. 2013) package. The sampler was run for 3000 steps using 32 walkers, with the first 225 steps in each chain (five times the integrated autocorrelation length, τ; Goodman & Weare 2010) discarded as burn-in. The resultant posterior distributions are shown in Figure 14. From the marginalised parameter distributions, we derived $T_{\rm eff} = 11\,100^{+2200}_{-1500}$ K for the WD, accounting for the uncertainties in reddening and an unknown $\log g$. As expected, poor constraints on $\log g$ are obtained from photometry alone, with spectroscopy in the quiescent phase being most useful to determine the value. Our derived temperature (11 000 K) for the WD in GOTO0650 is towards the lower end of the effective temperature distribution of WDs in CV systems (e.g. Pala et al. 2017), and it is directly comparable with a number of period bounce candidates, for instance QZ Lib (10 500 K; Pala et al. 2018) and EZ Lyn (12 000 K; Aviles et al. 2010). Stronger constraints on the effective temperature via near-UV photometry to constrain the Balmer jump or deep spectroscopy to probe the WD spectral features will be crucial to cement this clue towards the nature of GOTO0650. We assumed that we observed the WD, in which components from the discand accretion column may be present.

---

[11] https://github.com/mahollands/MR_relation

Table 5. Unabsorbed fluxes, photon index, and luminosity of GOTO0650 determined using EP FXT data.

Time (days)	Flux (erg s^{-1} cm^{-2})	Photon Index	Luminosity (erg s^{-1})
2.48	$10.6^{+2.0}_{-1.1} \times 10^{-14}$	3.23±0.29	$3.3^{+0.6}_{-0.3} \times 10^{30}$
6.02	$7.8^{+2.4}_{-1.0} \times 10^{-14}$	2.04±0.32	$2.4^{+0.8}_{-0.3} \times 10^{30}$
10.52	$8.2^{+3.7}_{-2.5} \times 10^{-14}$	1.92±0.33	$2.6^{+1.1}_{-0.7} \times 10^{30}$
14.88	$8.0^{+2.9}_{-1.1} \times 10^{-14}$	1.62±0.32	$2.5^{+0.9}_{-0.3} \times 10^{30}$
30.04	$4.2^{+2.9}_{-1.7} \times 10^{-14}$	1.50±0.49	$1.3^{+0.9}_{-0.5} \times 10^{30}$
30.56	$11.0^{+4.5}_{-3.3} \times 10^{-14}$	1.11±0.30	$3.4^{+1.4}_{-1.0} \times 10^{30}$
34.67	$12.3^{+3.4}_{-2.7} \times 10^{-14}$	1.10±0.22	$3.8^{+1.1}_{-0.8} \times 10^{30}$

Notes. Data were obtained at seven epochs. The luminosities were derived assuming a distance of 510 pc.
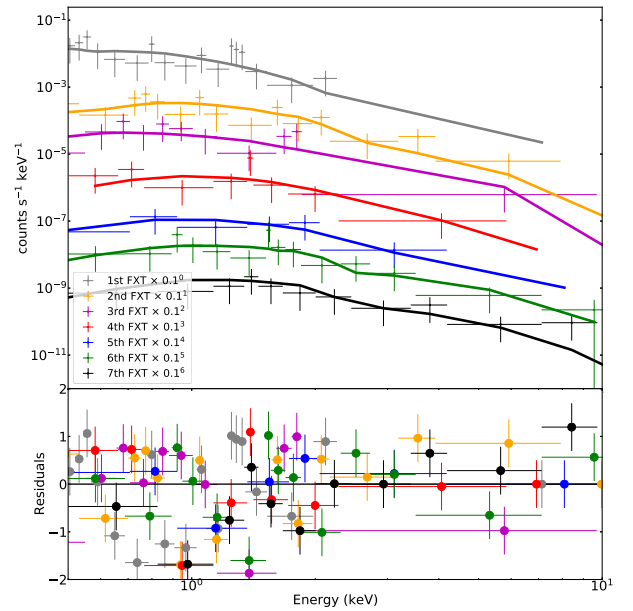
Fig. 15. Fits and residuals of the seven X-ray spectra taken using the EP FXT instrument using an absorbed power law.

4.6. X-ray fluxes and luminosity

In Section 3.3 we outlined the observations made using the EP and *Swift* X-ray telescopes. Using standard analysis tools, we determined the observed flux in the 0.5–10 keV band using an absorbed power law. We show the unabsorbed flux. The photon index and luminosity over time are shown in Table 5, and the spectral fits are presented in Figure 15. There is evidence that the X-ray flux was highest shortly after maximum optical brightness and then again between 30–35 d after discovery during the first main dip phase.

When we assume a distance of 510 pc, the X-ray luminosity of GOTO0650 is in the range 1.3–3.8×10^{30} erg s^{-1}. The slope of the power law was significantly steeper during the first epoch. X-ray observations of GW Lib and SSS J122222-311525 showed a decline in X-ray flux from maximum optical light (Neustroev et al. 2018). The X-ray luminosity of GOTO0650 is lower by an order of magnitude than that of SSS J1222.

We merged the seven epochs of *Swift* XRT data to obtain an event file with a combined exposure time of 6.96 ksec. From

this event file, we made an image using `xselect`[12]. We used the HEASoft tool `XIMAGE` and the routine `SOSTA` (which takes effects such as vignetting, exposure, and the point spread function into account) to determine a 3σ upper limit at the position of GOTO0650 of 2.65×10^{-3} count/s. Using `PIMMS`[13], we assumed a hydrogen column density of 3.9×10^{20} cm^{-2} (consistent with $A_V = 0.22$) and determined an unabsorbed flux (0.5–10 keV) of 9.7×10^{-14} for a photon index of 1.8 (the mean of that derived using EP data). The emission detected by the Einstein Probe is often below the upper limits obtained from the summed Swift XRT observations. There is no evidence for historical X-ray emission from GOTO0650 in a number of high-energy surveys. ROSAT All-Sky Survey (RASS; Voges et al. 1999) observations in 1990 yielded an upper limit of 2.2×10^{-13} erg s^{-1} cm^{-2} in the 0.2–2 keV band.

5. Discussion

With an outburst amplitude of ~8.5 mag, a likely orbital period of ~90 min, and ten echo outbursts, GOTO0650 shares all the characteristics of an WZ Sge-type accreting binary. The light curve overall appears to be similar to the 1996–1997 outburst of EG Cnc (Patterson et al. 1998). The recurrence time of the echo outbursts in GOTO0650 becomes shorter, and the amplitude decreases, with a slow increase in the inter-outburst quiescent brightness. The 1951 superoutburst identified in DASCH plates (see Figure 2) indicates that there was one outburst 73 years ago. Although we cannot discount that outbursts were missed in these intervening years, it does indicate a likely outburst recurrence time of many years or decades. WZ Sge and EG Cnc show outbursts every few decades.

5.1. Superhumps

One key observational property of WZ Sge binaries are the superhumps. At this stage, however, it is unclear which observations were made in the first week of the outburst and how sensitive they were to any superhump feature. The available AAVSO photometric coverage shows no significant periodicity prior to +13.8 d, but it does not robustly rule out low-amplitude periodicities. If superhumps were indeed absent, it is unusual that they were only detected two weeks after the outburst: AL Com, for instance, showed superhumps within the first week of an outburst in 1995 (Patterson et al. 1996). Osaki & Meyer (2002) showed that the absence of early superhumps might be due to the low inclination of the system, however, which might be reinforced by the low-EW narrowly separated double-peak profile seen in our quiescent spectrum.

5.2. Temperature of the white dwarf

Because of the long recurrence time between outbursts, WZ Sge systems are excellent objects for determining the temperature of the WD in the absence of accretion events and for determining the timescale of WD cooling (years) over the post outburst phase (e.g. Godon et al. 2006). We know that the temperature of the white dwarf in GOTO0650 in quiescence is approximately 10–13 kK (Section 4.5) but is likely to be two to three times hotter during the immediate post-peak epoch. Although the temperature is not especially well constrained, the WD could lie beyond

the cool edge of the WD instability strip (e.g. Van Grootel et al. 2012). It is therefore possible that GOTO0650 may pass through the WD instability strip as it cools. Observations of WZ Sge showed photometric pulsations around 28 s as it declined from outburst Welsh et al. (e.g. 2003). Because the period was not stable, it was not a signature of the WD rotation period. It remains unclear whether its origin is g-mode pulsations (low-frequency gravity-mode pulsations due to horizontal displacements of stellar gas) of the WD or due to channelled magnetic accretion onto the WD. Interestingly, Castro Segura et al. (2025) obtained multi-band high-cadence photometry of GOTO0650 during the decline from an echo outburst, and they identified a periodicity of 148.5±0.4 s that is markedly longer than what was seen for the WZ Sge pulsations. Castro Segura et al. (2025) outline possible origins for their observed periodicity.

5.3. Space density of CVs

Although there are many thousands of known or suspected CVs, their predicted space density differs from the number that is known. Pala et al. (2020) used Gaia data to identify all the known CVs out to a distance of 150 pc. The observed fraction of period bounce CVs in this sample is five times smaller at least than the predicted number. The superhump period and the narrow emission lines imply weak mass transfer and indicate that GOTO0650 is a candidate period bounce CV. Confirmation will require phase-resolved spectroscopy before the system has returned to quiescence, as it would then be too faint ($g = 21.8$). This is therefore a crucial component for understanding the GOTO0650 system.

5.4. Citizen science

Even in the age of widespread wide-field imaging surveys, the discovery of Galactic transient events with amplitudes >8 mag is relatively rare. Since they can be identified quickly and are likely to take some considerable time to return to quiescence, they provide a great opportunity for performing multi-wavelength observations during the event to study phenomena such as echo outbursts, which in turn give insight into how accretion discs can repeatedly switch from stable to unstable states.

These rapid requests for observations are not always possible on large telescopes. Citizen scientists are often able to spend entire nights observing a single source at very short notice, however, which generates high-quality data. A geographically distributed ensemble of these scientists can determine (as demonstrated by Figure 8) the evolution of the superhump period during the outburst, which can then be used to understand the conditions in the accretion disc and to test theoretical models.

The second key aspect for follow-up observations is spectroscopy. As demonstrated in our case, citizen scientists are able to obtain low-resolution spectroscopy even of relatively faint systems, which is more than adequate to reveal whether specific lines are in absorption or emission. However, 2 m class telescopes are generally required for higher-resolution spectroscopy of fainter targets such as GOTO650, which can reveal weak emission lines in absorption cores. Even higher resolution ($R \gtrsim 2000$) spectra from larger telescopes are required to search for radial velocity variations, which can constrain the masses of the binary components, and measure the orbital period to determine the evolutionary pathway of short-period binaries. Observations such as these are essential for us to determine whether objects such as GOTO0650 are indeed period bouncer systems that have evolved through the period minimum.

---

[12] https://heasarc.gsfc.nasa.gov/docs/software/ftools/xselect/
[13] https://heasarc.gsfc.nasa.gov/cgi-bin/Tools/w3pimms/w3pimms.pl

6. Conclusions

We presented the discovery of a very high-amplitude binary system, GOTO0650. We revealed that this is a WZ Sge system. This system was discovered, observed, and characterised by citizen scientists, which further underscores the vital contribution to variable star science routinely made by citizen scientists. Our intensive follow-up observations revealed an outburst light curve similar to the king of the echo outbursts EG Cnc (Patterson et al. 1998), and superhumps were only detected two weeks after the outburst. The spectra of GOTO0650 showed only one instance in which emission lines were detected and showed strong H emission only in emission, with very weak or non-detected He emission. The ten detected echo outbursts of GOTO0650 have a number of intriguing characteristics (rapidly decreasing recurrence timescales, a decreasing amplitude and duration, and an overall brightness increase in the low state). Continued photometric and spectroscopic observations of GOTO0650, in particular, high-resolution time-resolved spectroscopy, are required before the system returns to quiescence to constrain the radial velocities of the binary components and thus determine whether GOTO0650 is indeed a period bouncer.

Data availability

A machine-readable version of Table A.1 is available at the CDS via anonymous ftp to `cdsarc.cds.unistra.fr` (`130.79.128.5`) or via `https://cdsarc.cds.unistra.fr/viz-bin/cat/J/A+A/699/A8`.

References

Aviles, A., Zharikov, S., Tovmassian, G., et al. 2010, ApJ, 711, 389
Bédard, A., Bergeron, P., Brassard, P., & Fontaine, G. 2020, ApJ, 901, 93
Bellm, E. C., Kulkarni, S. R., Graham, M. J., et al. 2019, PASP, 131, 018002
Belloni, D., Schreiber, M. R., Pala, A. F., et al. 2020, MNRAS, 491, 5717
Bradley, L., Sipocz, B., Robitaille, T., et al. 2016, Astrophysics Source Code Library [record ascl:1609.011]
Brown, T. M., Baliber, N., Bianco, F. B., et al. 2013, PASP, 125, 1031
Castro Segura, N., Irving, Z. A., Vincentelli, F. M., et al. 2025, MNRAS, 541, L28
Chambers, K. C., Magnier, E. A., Metcalfe, N., et al. 2016, arXiv e-prints [arXiv:1612.05560]
Dey, A., Schlegel, D. J., Lang, D., et al. 2019, AJ, 157, 168
Dyer, M. J., Dhillon, V. S., Littlefair, S., et al. 2018, in Observatory Operations: Strategies, Processes, and Systems VII, Society of Photo-Optical Instrumentation Engineers (SPIE) Conference Series, 10704, 107040C
Dyer, M. J., Ackley, K., Jiménez-Ibarra, F., et al. 2024, in Ground-based and Airborne Telescopes X, eds. H. K. Marshall, J. Spyromilio, & T. Usuda, Society of Photo-Optical Instrumentation Engineers (SPIE) Conference Series, 13094, 130941X
Fitzpatrick, E. L. 1999, PASP, 111, 63
Foreman-Mackey, D., Hogg, D. W., Lang, D., & Goodman, J. 2013, PASP, 125, 306
Gaia Collaboration (Montegriffo, P., et al.) 2023, A&A, 674, A33
Gilliland, R. L., Kemper, E., & Suntzeff, N. 1986, ApJ, 301, 252
Godon, P., Sion, E. M., Cheng, F., et al. 2006, ApJ, 642, 1018
Goliasch, J., & Nelson, L. 2015, ApJ, 809, 80
Goodman, J., & Weare, J. 2010, Commun. Appl. Math. Comp. Sci., 5, 65
Grindlay, J., Tang, S., Los, E., & Servillat, M. 2012, in New Horizons in Time Domain Astronomy, eds. E. Griffin, R. Hanisch, & R. Seaman, IAU Symposium, 285, 29
Hardy, L. K., Butterley, T., Dhillon, V. S., Littlefair, S. P., & Wilson, R. W. 2015, MNRAS, 454, 4316
Hind, J. R. 1856, MNRAS, 16, 56
Hiroi, K., Moritani, Y., Nogami, D., et al. 2009, PASJ, 61, 697
Holberg, J. B., & Bergeron, P. 2006, AJ, 132, 1221
Horne, K., & Marsh, T. R. 1986, MNRAS, 218, 761
Howell, S. B., Nelson, L. A., & Rappaport, S. 2001, ApJ, 550, 897
Inight, K., Gänsicke, B. T., Breedt, E., et al. 2023, MNRAS, 524, 4867
Jensen, L. T., Poyner, G., van Cauteren, P., & Vanmunster, T. 1995, Messenger, 80, 43
Kato, T. 2015, PASJ, 67, 108
Kato, T., & Osaki, Y. 2013, PASJ, 65, 115
Kato, T., Nogami, D., Matsumoto, K., & Baba, H. 2004, PASJ, 56, S109
Killestein, T., Kelsey, L., Ramsay, G., et al. 2024a, ATel, 16842, 1

Killestein, T. L., Kelsey, L., Wickens, E., et al. 2024b, MNRAS, 533, 2113
Killestein, T., Pursiainen, M., Warwick, B., et al. 2024c, ATel, 16858, 1
Knigge, C., Baraffe, I., & Patterson, J. 2011, ApJS, 194, 28
Kochanek, C. S., Shappee, B. J., Stanek, K. Z., et al. 2017, PASP, 129, 104502
Kolb, U. 1993, A&A, 271, 149
Lallement, R., Vergely, J. L., Babusiaux, C., & Cox, N. L. J. 2022, A&A, 661, A147
Lang, D., Hogg, D. W., Mierle, K., Blanton, M., & Roweis, S. 2010, AJ, 139, 1782
Lomb, N. R. 1976, Ap&SS, 39, 447
Masci, F. J., Laher, R. R., Rusholme, B., et al. 2023, arXiv e-prints [arXiv:2305.16279]
McCully, C., Volgenau, N. H., Harbeck, D. R., et al. 2018, in Software and Cyberinfrastructure for Astronomy V, eds. J. C. Guzman, & J. Ibsen, Society of Photo-Optical Instrumentation Engineers (SPIE) Conference Series, 10707, 107070K
Meyer, F., & Meyer-Hofmeister, E. 2015, PASJ, 67, 52
Neustroev, V. V., Page, K. L., Kuulkers, E., et al. 2018, A&A, 611, A13
Osaki, Y., & Meyer, F. 2002, A&A, 383, 574
Pala, A. F., Gänsicke, B. T., Townsley, D., et al. 2017, MNRAS, 466, 2855
Pala, A. F., Schmidtobreick, L., Tappert, C., Gänsicke, B. T., & Mehner, A. 2018, MNRAS, 481, 2523
Pala, A. F., Gänsicke, B. T., Breedt, E., et al. 2020, MNRAS, 494, 3799
Patterson, J. 2011, MNRAS, 411, 2695
Patterson, J., Augusteijn, T., Harvey, D. A., et al. 1996, PASP, 108, 748
Patterson, J., Kemp, J., Skillman, D. R., et al. 1998, PASP, 110, 1290
Patterson, J., Masi, G., Richmond, M. W., et al. 2002, PASP, 114, 721
Piascik, A. S., Steele, I. A., Bates, S. D., et al. 2014, in Ground-based and Airborne Instrumentation for Astronomy V, eds. S. K. Ramsay, I. S. McLean, & H. Takami, Society of Photo-Optical Instrumentation Engineers (SPIE) Conference Series, 9147, 91478H
Prochaska, J., Hennawi, J., Westfall, K., et al. 2020, J. Open Source Softw., 5, 2308
Ridden-Harper, R., Tucker, B. E., Garnavich, P., et al. 2019, MNRAS, 490, 5551
Roming, P. W. A., Kennedy, T. E., Mason, K. O., et al. 2005, Space Sci. Rev., 120, 95
Scargle, J. D. 1982, ApJ, 263, 835
Schreiber, M. R., Belloni, D., & Schwope, A. D. 2024, A&A, 682, L7
Shappee, B. J., Prieto, J. L., Grupe, D., et al. 2014, ApJ, 788, 48
Shears, J. 2018, J. Brit. Astron. Assoc., 128, 75
Shingles, L., Smith, K. W., Young, D. R., et al. 2021, TNSAN, 7, 1
Steeghs, D., Galloway, D. K., Ackley, K., et al. 2022, MNRAS, 511, 2405
Steele, I. A., Smith, R. J., Rees, P. C., et al. 2004, in Ground-based Telescopes, eds. J. Oschmann, & M. Jacobus, Society of Photo-Optical Instrumentation Engineers (SPIE) Conference Series, 5489, 679
Szkody, P., Henden, A., Fraser, O., et al. 2004, AJ, 128, 1882
Tampo, Y., Isogai, K., Kojiguchi, N., et al. 2021, PASJ, 73, 753
Tampo, Y., Kato, T., Kojiguchi, N., et al. 2023, PASJ, 75, 619
Tonry, J. L., Stubbs, C. W., Lykke, K. R., et al. 2012, ApJ, 750, 99
Tonry, J. L., Denneau, L., Heinze, A. N., et al. 2018, PASP, 130, 064505
Tovmassian, G., Gänsicke, B. T., Echevarria, J., Zharikov, S., & Ramirez, A. 2022, ApJ, 939, 14
Tremblay, P. E., Bergeron, P., & Gianninas, A. 2011, ApJ, 730, 128
Van Grootel, V., Dupret, M. A., Fontaine, G., et al. 2012, A&A, 539, A87
Vergely, J. L., Lallement, R., & Cox, N. L. J. 2022, A&A, 664, A174
Voges, W., Aschenbach, B., Boller, T., et al. 1999, A&A, 349, 389
Warner, B. 2003, Cataclysmic Variable Stars (Cambridge University Press)
Welsh, W. F., Sion, E. M., Godon, P., et al. 2003, ApJ, 599, 509
Yuan, W., Zhang, C., Chen, Y., & Ling, Z. 2022, in Handbook of X-ray and Gamma-ray Astrophysics, eds. C. Bambi, & A. Sangangelo, 86

[1] Department of Physics & Astronomy, University of Turku, Vesilinnantie 5, Turku FI-20014, Finland
[2] Department of Physics, University of Warwick, Gibbet Hill Road, Coventry CV4 7AL, UK
[3] Armagh Observatory & Planetarium, College Hill, Armagh BT61 9DG, UK
[4] School of Physics, Kane Building, University College Cork, Cork, Ireland
[5] Institute of Astronomy and Kavli Institute for Cosmology, University of Cambridge, Madingley Road, Cambridge CB3 0HA, UK
[6] Astrophysics Research Cluster, School of Mathematical and Physical Sciences, University of Sheffield, Sheffield S3 7RH, UK
[7] Institute of Cosmology and Gravitation, University of Portsmouth, Portsmouth PO1 3FX, UK
[8] Kilonova Seekers c/o Zooniverse, Department of Physics, University of Oxford, Denys Wilkinson Building, Keble Road, Oxford OX1 3RH, UK
[9] Institute of Plant Physiology and Genetics, Bulgarian Academy of Sciences, Acad. G. Bontchev Str., Bl.23, Sofia 1113, Bulgaria
[10] American Association of Variable Star Observers, 185 Alewife Brook Parkway, Suite 410, Cambridge, MA 02138, USA
[11] Variable Stars South, Royal Astronomical Society of New Zealand, P O Box 3181, Wellington, New Zealand
[12] British Astronomical Association Variable Star Section, Burlington House, Piccadilly, London W1J 0DU, UK
[13] School of Physics & Astronomy, Monash University, Clayton VIC 3800, Australia
[14] Instituto de Astrofísica de Canarias, E-38205 La Laguna, Tenerife, Spain
[15] School of Physics & Astronomy, University of Leicester, University Road, Leicester LE1 7RH, UK
[16] National Astronomical Research Institute of Thailand, 260 Moo 4, T. Donkaew, A. Maerim, Chiangmai 50180, Thailand
[17] Jodrell Bank Centre for Astrophysics, Department of Physics and Astronomy, The University of Manchester, Manchester M13 9PL, UK
[18] Department of Physics, Royal Holloway – University of London, Egham Hill, Egham TW20 0EX, UK
[19] Centre for Advanced Instrumentation, University of Durham, DH1 3LE Durham, UK
[20] School of Sciences, European University Cyprus, Diogenes street, Engomi, 1516 Nicosia, Cyprus
[21] Department of Astronomy, Tsinghua University, Beijing 100084, China
[22] Physics Department, Tsinghua University, Beijing 100084, China
[23] School of Physics and Astronomy, Beijing Normal University, Beijing 100875, China
[24] Institute for Frontier in Astronomy and Astrophysics, Beijing Normal University, Beijing 102206, China
[25] Yunnan Observatories, Chinese Academy of Sciences, Kunming 650216, China
[26] Key Laboratory for the Structure and Evolution of Celestial Objects, Chinese Academy of Sciences, Kunming 650216, China
[27] Key Laboratory of Particle Astrophysics, Institute of High Energy Physics, Chinese Academy of Sciences, 100049 Beijing, China
[28] National Astronomical Observatories, Chinese Academy of Sciences, Beijing 100101, China
[29] School of Astronomy and Space Science, University of Chinese Academy of Sciences, Beijing 100049, China
[30] Department of Earth and Environmental Sciences, The University of Manchester, Williamson Building, Oxford Road, Manchester M13 9PL, UK
[31] Royal Astronomical Society, Burlington House, Piccadilly, London W1J 0BQ, UK
[32] Physical Sciences Group, Siena Academy of Sciences, Piazzetta Silvio Gigli 2, 53100 Siena, Italy
[33] Astronomical Soc. of Southern Africa, c/o SAAO POBox 9, Observatory 7935 CT Rep, South Africa
[34] Institute for Advanced Physical Studies, 111 'Tsarigradsko shose' Blvd, Sofia 1784, Bulgaria
[35] AstroLAB IRIS, Provinciaal Domein 'De Palingbeek', Verbrandemolenstraat 5, 8902 Zillebeke, Ieper, Belgium
[36] Vereniging Voor Sterrenkunde (VVS), Oostmeers 122 C, 8000 Brugge, Belgium
[37] Groupe Européen d'Observations Stellaires (GEOS), 23 Parc de Levesville, 28300 Bailleau l'Evêque, France
[38] Bundesdeutsche Arbeitsgemeinschaft für Veränderliche Sterne e.V. (BAV), Munsterdamm 90, 12169 Berlin, Germany
[39] Center for Backyard Astrophysics, New York, NY, USA
[40] Hankasalmi Observatory, Hankasalmi, Finland
[41] Burke-Gaffney Observatory, Saint Mary's University, 923 Robie Street, Halifax, NS B3H 3C3, Canada
[42] Polaris Observatory, Hungarian Astronomical Association, Laborc utca 2/c, 1037 Budapest, Hungary

Appendix A: Additional table

Table A.1. All obtained photometry of GOTO0650 presented in this work.

Date (MJD)	Phase (d)	Filter	Magnitude (AB)	Error	Telescope
60587.15	+0.0	L	13.37	0.00	GOTO
60587.55	+0.4	u	13.31	0.02	LCO 0.4m
60587.55	+0.4	r	13.37	0.01	LCO 0.4m
60587.55	+0.4	i	13.55	0.01	LCO 0.4m
60587.55	+0.4	z	13.83	0.04	LCO 0.4m
			⋮		
60756.09	+168.9	r	19.62	0.18	LCO 0.4m

Notes. Magnitudes are uncorrected for Galactic extinction. A machine-readable version of this table is available at the CDS.